Article No. jmbi.1999.3492 available online at http://www.idealibrary.com on IDEAL® J. Mol. Biol. (2000) 296, 341–349

JMB

COMMUNICATION

Structure of Human Neutral Endopeptidase (Neprilysin) Complexed with Phosphoramidon

Christian Oefner, Allan D'Arcy, Michael Hennig, Fritz K. Winkler and Glenn E. Dale*

Pharma Preclinical Research
F. Hoffmann-La Roche Ltd.
CH-4070, Basel, Switzerland

Neutral endopeptidase is a mammalian type II integral membrane zinc-containing endopeptidase, which degrades and inactivates a number of bioactive peptides. The range of substrates cleaved by neutral endopeptidase *in vitro* includes the enkephalins, substance P, endothelin, bradykinin and atrial natriuretic factor. Due to the physiological importance of neutral endopeptidase in the modulation of nociceptive and pressor responses there is considerable interest in inhibitors of this enzyme as novel analgesics and anti-hypertensive agents. Here we describe the crystal structure of the extracellular domain (residues 52-749) of human NEP complexed with the generic metalloproteinase inhibitor phosphoramidon at 2.1 Å resolution. The structure reveals two multiply connected folding domains which embrace a large central cavity containing the active site. The inhibitor is bound to one side of this cavity and its binding mode provides a detailed understanding of the ligand-binding and specificity determinants.

© 2000 Academic Press

Keywords: enkephalinase; metalloprotease; phosphoramidon; X-ray structure; endothelin converting enzyme

*Corresponding author

Neutral endopeptidase (NEP) (EC 3.4.24.11), also known as neprilysin, enkephalinase, NEP, CALLA or CD10, is a membrane-bound zinc-dependent endopeptidase originally extracted and purified from the brush border of rabbit kidney (Kerr & Kenny, 1974). This ectoenzyme is widely distributed in mammalian tissues and is involved in the inactivation of a variety of signaling peptides (Erdos & Skidgel, 1989; Roques *et al.*, 1993; Turner & Tanzawa, 1997). NEP has been implicated in the regulation of opioid peptide action through the degradation of endogenously released enkephalins (Roques *et al.*, 1980). Furthermore, it is involved in the physiological degradation of the peptides modulating blood pressure, such as the cardiac hormone atrial natriuretic peptide (ANP), bradykinin and endothelin. There is great interest in the identification of novel inhibitors of NEP for application in clinical treatment (Abassi *et al.*, 1992; Kenny & Stephenson, 1988; Pham *et al.*, 1993). Potent inhibitors of NEP have been synthesized which produce a pharmacological response through increase in opioid or vasoactive peptide levels, indicating their therapeutic potential as novel analgesics or antihypertensive agents (Burnett, 1999; Chen *et al.*, 1998; Robl *et al.*, 1997, 1999; Roques & Beaumont, 1990).

The primary sequence of NEP has been determined by cloning its cDNA from several species (Devault *et al.*, 1987; Malfroy *et al.*, 1987, 1988). NEP is the prototype of a group of metallopeptidases which includes the endothelin-converting enzymes (ECE-1 and ECE-2), the erythrocyte surface antigen KELL, and the PEX gene product. They belong to the M13 subfamily of mammalian neutral endopeptidases and consist of a short N-terminal cytoplasmic domain, followed by a single transmembrane helix, and a large C-terminal extracellular domain that contains the active site (The HYP consortium, 1995; Emoto & Yanagisawa, 1995; Lee *et al.*, 1991; Shimada *et al.*, 1994). The extracellular domain of NEP contains 12 cysteine residues, all involved in disulfide bridges, ten of which are conserved in ECE,

Abbreviations used: NEP, neutral endopeptidase; ANP, atrial natriuretic peptide; TLN, thermolysin; SNEP, soluble extracellular domain of human neutral endopeptidase; NAG, *N*-acetyl-glucosamine.

E-mail address of the corresponding author: glenn.dale@roche.com

0022-2836/00/020341–9 $35.00/0

© 2000 Academic Press

Zydus EX1045
U.S. Patent No. 12,233,106

KELL, and PEX (Figure 1). The overall homology between NEP and ECE-1, ECE-2, KELL and PEX is 35%, 30%, 31%, and 25%, respectively, but increases to 51%, 44%, 43%, and 39% if only the 250 C-terminal residues are considered. This degree of similarity is sufficient to indicate that these proteins share a common origin and a similar fold.

The catalytic properties of NEP resemble those of a group of zinc-dependent bacterial endopeptidases of which thermolysin (TLN) is the best characterized. Early structure-activity studies showed that TLN and NEP cleave the peptide bond of their substrates at the amino side of hydrophobic residues and that both enzymes are inhibited by the same type of molecules, such as phosphoramidon and thiorphan, with the same stereochemical dependence (Benchetrit *et al.*, 1987; Fulcher *et al.*, 1982; Hersh & Morihara, 1986). Although there is very limited homology between the primary sequences of mammalian and bacterial enzymes, they are characterized by two consensus sequences HExxH and ExxxD, involved in zinc binding and catalysis (Matthews, 1988). Hydrophobic cluster analysis suggested important similarities in their active sites and putative residues

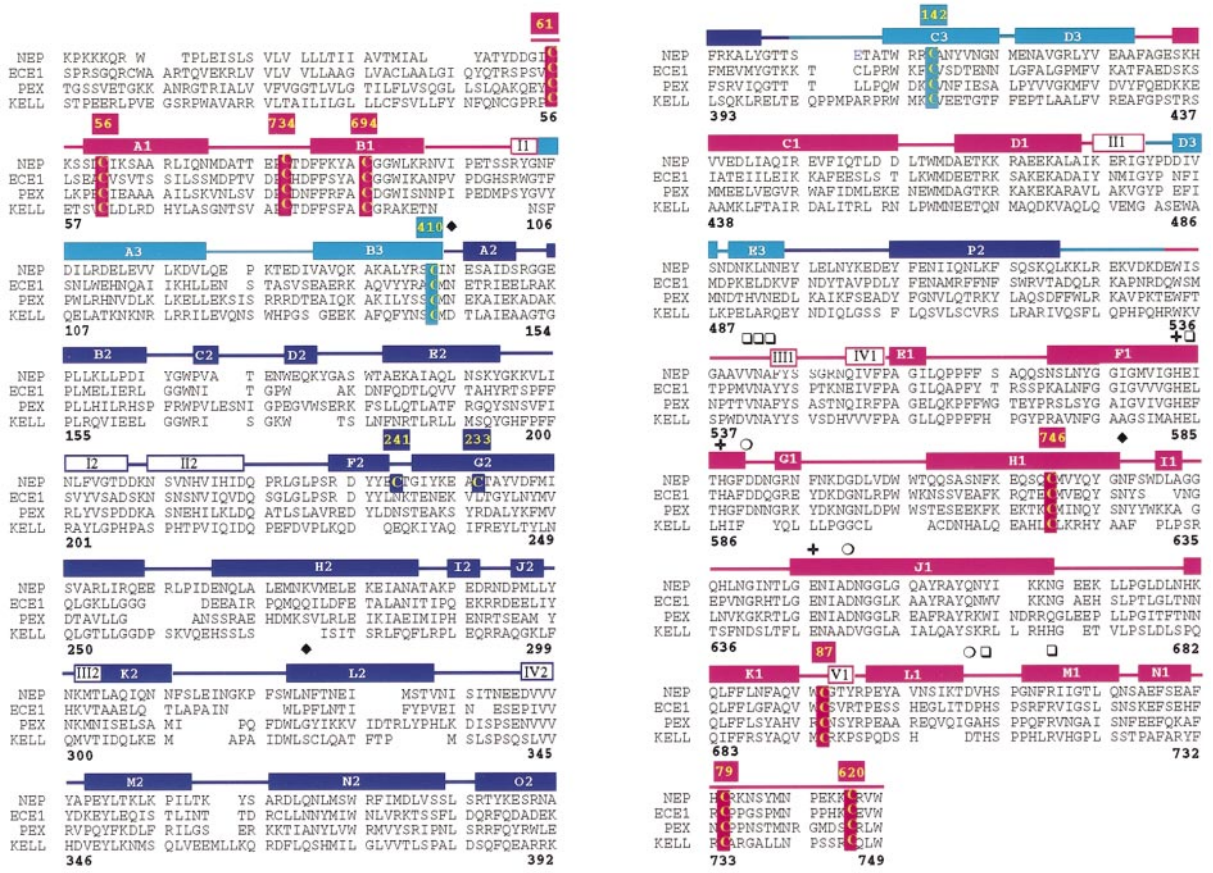


Figure 1. Multiple sequence alignment of selected mammalian membrane metallopeptidases NEP, ECE, KELL and PEX. The α-helices, filled cylinders, β-strands, open cylinders, are drawn above the sequence. Coloring as indicated in Figure 2. Zinc-binding residues, crosses; ligand-binding residues; open squares. Residues implicated in the stabilization of the active site are labeled by circles and glycosylation sites are indicated with diamonds. Cysteine residues and their respective disulfide-bond partners are indicated. Protein expression, purification and crystallization will be described in detail elsewhere (Dale *et al.*, unpublished results). Briefly, the extracellular domain of human NEP (residues 52-749) was cloned into pPICZα-C to create a fusion with the α-mating factor signal sequence and protein produced in the yeast *Pichia pastoris* GS115. Protein expression was accomplished using YP medium with 3% methanol. The secretion level of sNEP was modest at 10 mg/l. The sNEP could be purified to homogeneity using five chromatographic steps. The N-terminal sequence of purified sNEP indicated that the protein was efficiently processed by the STE13 signal peptidase. The kinetic properties of sNEP were similar to that of the native enzyme (data not shown). Mass spectral analysis of the purified protein resulted in a mass of 92,186 Da (predicted molecular mass is 80,086 Da) indicating that the protein is significantly glycosylated. Treatment of sNEP with Endo-F1 glycosidase resulted in a decrease in approximately 10 kDa giving a final mass of 81,369 Da indicating that a small degree of glycosylation remained. Light-scattering analysis of both sNEP and the de-glycosylated sNEP showed a narrow unimodal size distribution suggesting that they were suitable for crystallization trials.

involved in zinc coordination, catalysis and substrate binding have been identified in NEP by site-directed mutagenesis experiments (Benchetrit *et al.*, 1988; Devault *et al.*, 1988a,b; Dion *et al.*, 1993, 1995; Le Moual *et al.*, 1991, 1994). In the absence of structural information for any member of the neprilysin family, the observed three-dimensional fold for the TLN family has been used to generate a model of the active site region of NEP for the design of new NEP inhibitors (Gaucher *et al.*, 1999; Ksander *et al.*, 1997a,b; Tiraboschi *et al.*, 1999).

In order to aid in the design of potent and selective inhibitors of this structural class, we have solved the three-dimensional structure of human NEP by X-ray crystallography. The soluble extracellular domain (D52 to W749) of human NEP (sNEP) was expressed in the yeast *Pichia pastoris* and the protein purified to homogeneity (Figure 1). Crystals could be obtained for the Endo-F1 glycosidase treated enzyme in the presence of the inhibitor phosphoramidon (*N*-(α-L-rhamnopyranosyl-oxyhydroxy-phosphinyl)-L-leucyl-L-tryptophan), a metabolite produced by *Streptomyces tanashiensis*. The structure was solved by the multiple isomorphous replacement method and refined to a crystallographic *R*-factor of 19.5% ($R_{free} = 24.2\%$) at 2.1 Å resolution (Figure 2). Data collection and refinement statistics are summarized in Table 1.

The overall shape of the monomeric ectodomain is an ellipsoid with a major axis of 95 Å and minor axes of approximately 55 Å. It is composed of two largely α-helical domains which can be considered as two lobes connected by intertwining polypeptide segments. A cartoon depicting the overall fold of human sNEP together with the secondary structure assignment is shown in Figure 3. The larger N-terminal domain (domain 1), which follows the trans-membrane anchor of the mature enzyme is 321 residues long and consists of three non-consecutive polypeptide segments (Figure 3). The residues essential for zinc coordination and catalysis are located within this domain. It is structurally most closely related to other zinc metalloproteases such as TLN, bacterial metallo-elastase and the neutral protease from *Bacillus cereus*. The smaller second domain (domain 2) is 286 residues long and composed of two non-consecutive polypeptide segments and shows a weak structural similarity with glycosyl hydrolase (Tews *et al.*, 1996). The enzyme has six disulfide bridges, five of which are conserved among the other members of the mammalian membrane metallopeptidase family (Figure 1). Four of these are located within the catalytic domain 1, a single disulfide bridge is found within the inter-domain linker fragments, and the non-conserved disulfide bond is present within domain 2. Unlike ECE, which exists as a disulfide-linked homodimer, sNEP is a monomer in solution. However, when E403, located on the surface in the linker region, is mutated to a cysteine residue (C412 in ECE) it results in the formation of a disulfide-bridged homodimer (Hoang *et al.*, 1997). *N*-Glycosylation on N144, N304 and N627 is confirmed by electron density consistent with a single *N*-acetyl-glucosamine (NAG) moiety.

Together with four inter-domain linker fragments both domains form a central, roughly spherical cavity, which bears the active site of the enzyme (Figures 3(a) and 4). The cavity has a diameter of approximately 20 Å and is accessible *via* a small, circular opening formed primarily by charged residues. One of the main differences between the mammalian metallopeptidases of the neprilysin family and the bacterial proteases is that the majority of the natural substrates of NEP are restricted to about 3000 Da. This selectivity is possibly due to the presence of domain 2 (not present in TLN), which restricts the active site access and thus functions as a molecular sieve. The inhibitor phosphoramidon is nestled in the interior of the cavity and binds near the highly conserved residues of the consensus sequences ^{583}HExxH^{687} and ^{646}ExxxD^{650} and the residues of the ^{542}NAFY^{545} motif (Figures 1 and 5). The residues belong to the zinc-binding helix F1, the helix J1 forming the

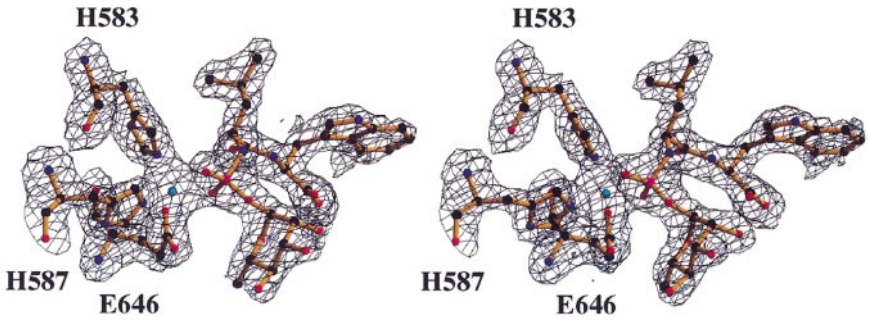


Figure 2. An $F_o - F_c$ omit electron-density map of phosphoramidon, zinc and the three metal binding ligands of the protein (H583, H586 and E646), calculated with phases from the refined model at 2.1 Å resolution. The map is contoured at 3σ.

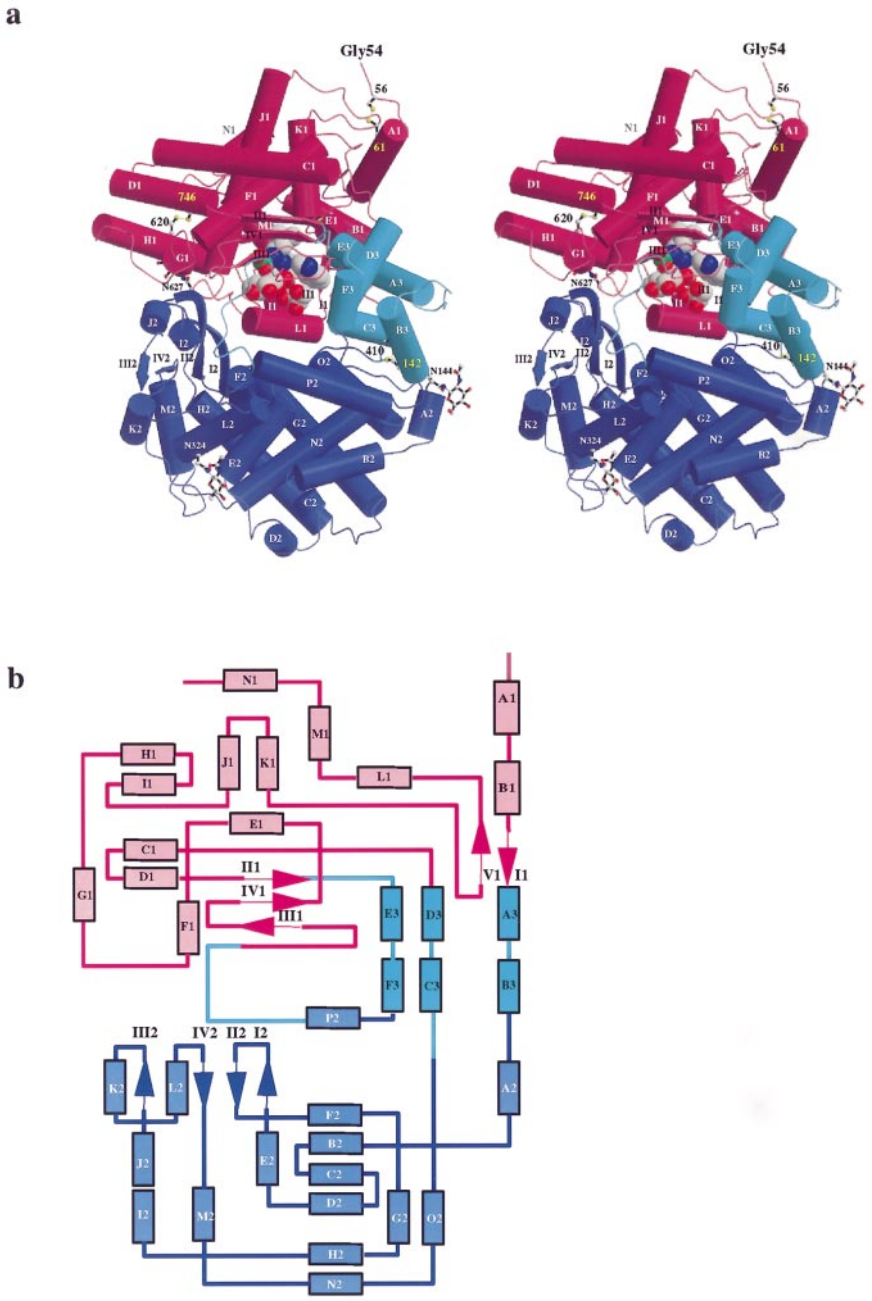


Figure 3. Ribbon plot and topology of sNEP complexed with phosphoramidon. (a) Stereoview of a cartoon model of human neprilysin, showing the catalytic domain 1, violet; the smaller domain 2, blue; and the three inter-domain linker fragments, cyan. The transition-state mimetic phosphoramidon is shown in CPK representation. Glycosylation sites and disulfide bonds are indicated. (b) Topological diagram of sNEP colored as above. Arrows denote strands and cylinders indicate helices numbered as in Figure 1.

base of the active site cleft, and β-strand III1 which acts as a cap holding the well-ordered inhibitor in the active site (Figure 5) (Sansom *et al.*, 1998).

The zinc ion is coordinated in an approximately tetrahedral geometry, as observed in TLN. Its binding involves a single oxygen atom (O1) of the tetrahedral N-phosphoryl moiety of the inhibitor with an inter-atomic distance of 1.93 Å, as well as three ligands from the protein, H583 (2.03 Å), H587 (2.01 Å), and E646 (1.96 Å) (Figure 5). The side-chains of D590 and D650 appear to be part of two Asp-His-Zinc triads, which involve H587 and H583 on the N and C-terminal site of the N-phosphoryl moiety, respectively. The latter triad is believed to be involved in the precise positioning of the zinc ion for catalysis (Le Moual *et al.*, 1994). A similar role can be expected for the N-terminal triad, which is conserved in all members of the neprilysin family. The side-chain of H711 is hydrogen bonded to the zinc ligand of the inhibitor and

Table 1. Crystallographic data and refinement statistics

Data sets (soaking conditions)	Native-1	Native-2	$EuCl_3$ (3 mM, 28 hours)	Thiomersal (5 mM, 120 hours)	$K_3UO_2F_5$ (2.5 mM, 144 hours)
Data collection					
Exposure time/frame (s)	900	120	500	600	600
Angular increment per frame (deg.)	0.5	1.0	0.5	0.5	0.5
Total rotation range (deg.)	75	61	41.5	58.5	55
Crystal to detector distance (mm)	180	360	200	200	200
Unit cell parameters *a* and *c* (Å)	107.6, 112.8	107.6, 112.8	107.8, 112.5	107.8, 112.8	107.7, 112.8
Data reduction					
Maximum resolution (Å)	2.44	2.00	2.44	2.44	2.44
Number of measurements	91.966	189.020	65.138	82.229	65.005
Number of unique reflections	26.702	49.828	26.578	26.761	25.817
Completeness (%)[a]	93.7 (79.9)[a]	99.4 (98.9)[a]	93.5 (92.3)[a]	93.5 (95.7)[a]	90.7 (95.5)[a]
R_{sym} [b]	9.6 (37.4)	5.3 (30.1)	11.5 (36.5)	6.6 (20.8)	8.21(37.5)
Heavy-atom refinement parameters					
Figure of merit (acentric/centric)	0.38/0.42				
R_{cullis} [c] (acentric/centric)			0.84/0.48	0.75/0.78	0.89/0.88
Phasing power[d] (acentric/centric)			1.05/0.86	1.07/0.76	0.97/0.79
Refinement statistics					
Resolution range (Å)	20-2.1				
R_{cryst} (R_{free}) (%)[e]	19.5 (24.2)				
Number of protein atoms[f] (mean *B* in Å^2)	5595 (29.1)				
Number of water molecules	465				
Number of ligand atoms (mean *B* in Å^2)	37 (20.8)				
Number of glycerol atoms (mean *B* in Å^2)	6 (44.9)				
Number of NAG atoms (mean *B* in Å^2)	42 (48.9)				
rmsd[g] bonds (Å^2)	0.009				
rmsd angles (deg.)	1.48				

[a] Values in parentheses are statistics for highest resolution bin.

[b] $R_{sym} = \Sigma_h \Sigma_i |I_i(h) - \langle I(h)\rangle| / \Sigma_h \Sigma_i I_i(h)$, where $I_i(h)$ and $\langle I(h)\rangle$ are the *i*th and mean measurement of the intensity of reflection *h*.

[c] $R_{cullis} = \Sigma_h |F_D(h) - |F_N(h) + |F_H(h)|| / \Sigma_h |F_D(h) - F_N(h)|$, where $F_H(h)$, $F_D(h)$ and $F_N(h)$ are the heavy atom, derivative and native structure factor amplitudes of reflection *h*.

[d] Phasing power $= \Sigma_h F_H(h) / \Sigma_h |F_D(h) - |F_N(h) + F_H(h)||$.

[e] $\Sigma_h ||F_{obs}| - |F_{calc}|| / \Sigma_h |F_{obs}|$, where $|F_{obs}|$ and $|F_{calc}|$ are the observed and calculated structure factor amplitudes for the reflection *h*, applied to the working (R_{cryst}) and test (R_{free}) sets, respectively.

[f] Non-hydrogen atoms, only.

[g] rmsd: root-mean-square deviation from mean.

A binary complex of the Endo-F1 glycosidase treated sNEP at 20 mg/ml and the inhibitor phoshoramidon at a concentration of 1 mM was formed. Crystals of the inhibited protein complex were obtained by vapor diffusion with 25% PEG 3350, 200 mM ammonium sulfate 100 mM bis-Tris at pH 7.5 as the precipitating agent. Crystals belong to the trigonal space group $P3_221$ with one molecule in the asymmetric unit. All crystals were flash frozen in a cryoprotectant solution corresponding to the reservoir condition containing 30% (v/v) glycerol and measured at 120 K. All data sets, except Native-2, were measured with CuKα radiation provided from a NONIUS FR591 rotating anode generator equipped with an OSMIC mirror system, recorded on a MAR-Research image plate area detector and evaluated with the XDS software (Kabsch, 1988). The Native-2 data set, used for refinement, was collected at the Swiss-Norwegian beam line (SNBL) at the European Synchrotron Radiation Facility (ESRF, Grenoble) on a MAR image plate at 0.86633 Å. Data were processed and scaled with DENZO and SCALEPACK (Otwinowski, 1993). All data sets were further analyzed with the CCP4 program suite (CCP4, 1994). A $EuCl_3$ derivative was solved from the isomorphous amplitude differences relative to Native-1 using the program SHELXS-97 (Sheldrick *et al.*, 1993). Three sites were identified and initial phases obtained from the isomorphous and anomalous differences of this derivative were used to solve a mercury and a uranyl derivative by difference Fourier methods. All heavy atom refinement and phasing was performed with the program SHARP (de La Fortelle & Bricogne, 1997). The initial SHARP electron density was modified and further improved with the program SOLOMON by applying iterative rounds of solvent-flipping and a final cycle of solvent-flattening using a solvent content of 56% (Abrahams & Leslie, 1996). This lead to a traceable electron density for about 90% of the structure at 2.5 Å resolution. Model building was performed with the in-house graphics program MOLOC, stereochemically restrained positional and temperature-factor refinement was done with CNS 0.5 against the amplitude based maximum likelihood target ''MLF1'', using parameters for ideal stereochemistry as described by Engh & Huber and a bulk solvent correction (Brünger *et al.*, 1998; Engh & Huber, 1991; Gerber, 1992; Jiang & Brünger, 1994; Kostrewa, 1997). Iterative rounds of model building and refinement lead to a model (lacking the N-terminal two residues D52 and D53) with excellent stereochemistry as examined by PROCHECK and converged to an *R*-factor of 0.194 using all data in the resolution range between 20.0 and 2.1 Å (42,045 reflections) with an R_{free} of 0.242 (2210 reflections) (Brünger, 1992; Laskowski *et al.*, 1993). All residues fall within the allowed regions of the Ramachandran Plot, with the exception of L199, which has a clearly defined backbone conformation. All Figures were generated with the programs MOLSCRIPT, RASTER3D, or GRASP (Kraulis, 1991; Merrit & Bacon, 1997; Nicholls & Honig, 1992).

has been implicated in the stabilization of the transition state (Dion *et al.*, 1995). Furthermore, this residue interacts with D709 and stabilizes a complex hydrogen bonding network, similar to that observed in TLN. This network also involves the residues E584, R717, as well as the tri-peptide ^{541}VNA^{543}. In the crystal structure E584 is hydrogen bonded to the second oxygen

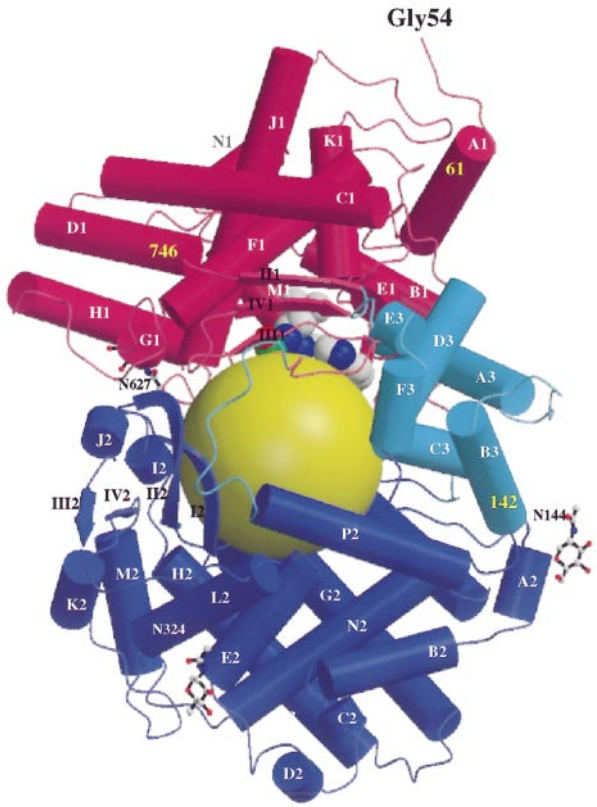


Figure 4. Ribbon plot of sNEP depicting the volume of the active site cavity.

atom of the tetrahedral N-phosphoryl moiety of the inhibitor (O2) with an inter-atomic distance of 2.73 Å and is in position to be involved in catalysis by polarizing the attacking water molecule (Devault *et al.*, 1988a). The side-chain of R717 participates in a salt bridge with D650 and plays a role in substrate hydrolysis and inhibitor binding (Marie-Claire *et al.*, 1997). It interacts with the inhibitor by forming a hydrogen bond with the carbonyl oxygen atom of the L-leucyl residue in the P_1' position. Additionally, the carbonyl oxygen atom of A543 is hydrogen bonded with the peptide amide group of the P_1' residue of phosphoramidon. The side-chain of N542 forms two hydrogen bonds with the NH and CO groups of the P_2' residue of the inhibitor with hydrogen-bonding distances of 3.27 Å and 3.20 Å, respectively, and thus plays an analogous role to that of N112 in TLN (Dion *et al.*, 1995). The indole NH of the L-tryptophan residue is hydrogen bonded to the main-chain carbonyl group of V541 (2.83 Å).

The rhamnose moiety of the P_1 residue of the inhibitor is mainly exposed to solvent, leaving 80 % of the surface of phosphoramidon in direct contact with the enzyme (Figure 5). This reflects the minor stabilizing role of the S_1 subsite expected by the slight increase in affinity of inhibitors with a P_1 side-chain (Gaucher *et al.*, 1999; Ksander *et al.*, 1997a,b). The absence of a stringent specificity for the S_1 subsite is in contrast to that observed for the binding site of the P_1' residue. The S_1' subsite of sNEP forms a large hydrophobic pocket that interacts preferentially with aromatic or large hydrophobic moieties (Tiraboschi *et al.*, 1999). It is formed by the side-chains of F106, I558, F563, M579, V580, V692 and W693. This subsite has a volume of approximately 220 A^3 and is only partially filled by the L-leucyl side-chain of the inhibitor. The indole moiety of the P_2' residue of the inhibitor is in van der Waals contact to the side-chain of F106. The S_2' subsite is large and extends to the solvent across the linker helix A3 towards the side-chains of R102, D107 and R110. This confirms the observation that the S_2' subsite of sNEP has reduced specificity and can accommodate bulky side-chains. None of these charged residues is involved in inhibitor binding. Moreover, the guanidinium group of both arginine residues is disordered in the otherwise well-defined active site. This is consistent with the role of R102 in substrate binding believed to be dependent on the geometry and the nature of the P_2' residue (Kim *et al.*, 1992). Interestingly, no residue of domain 2 is involved in inhibitor binding or subsite formation.

This is, to our knowledge, the first three-dimensional structure of a member of this pharmacologically important family of proteins. Among the wide range of biologically active peptide substrates for NEP, the enkephalins and the atrial natriuretic peptide have assumed greatest significance. They reflect the important role of this membrane peptidase in the modulation of nociceptive and pressor responses which has stimulated considerable interest in inhibitors of this enzyme to treat a variety of disease states including acute pain and hypertension. In the background of this rich biological context further understanding of NEP is poised to benefit from this structural study. The information provided by the three-dimensional structure presents an attractive challenge to increase the potency and selectivity of known inhibitor classes through docking studies. Moreover, this structure provides a tool for further characterization of other members of the neprilysin subfamily, such as ECE.

Protein Data Bank accession numbers

The NEP coordinates have been deposited in the RCSB Protein Data Bank (PDB code 1DMT).

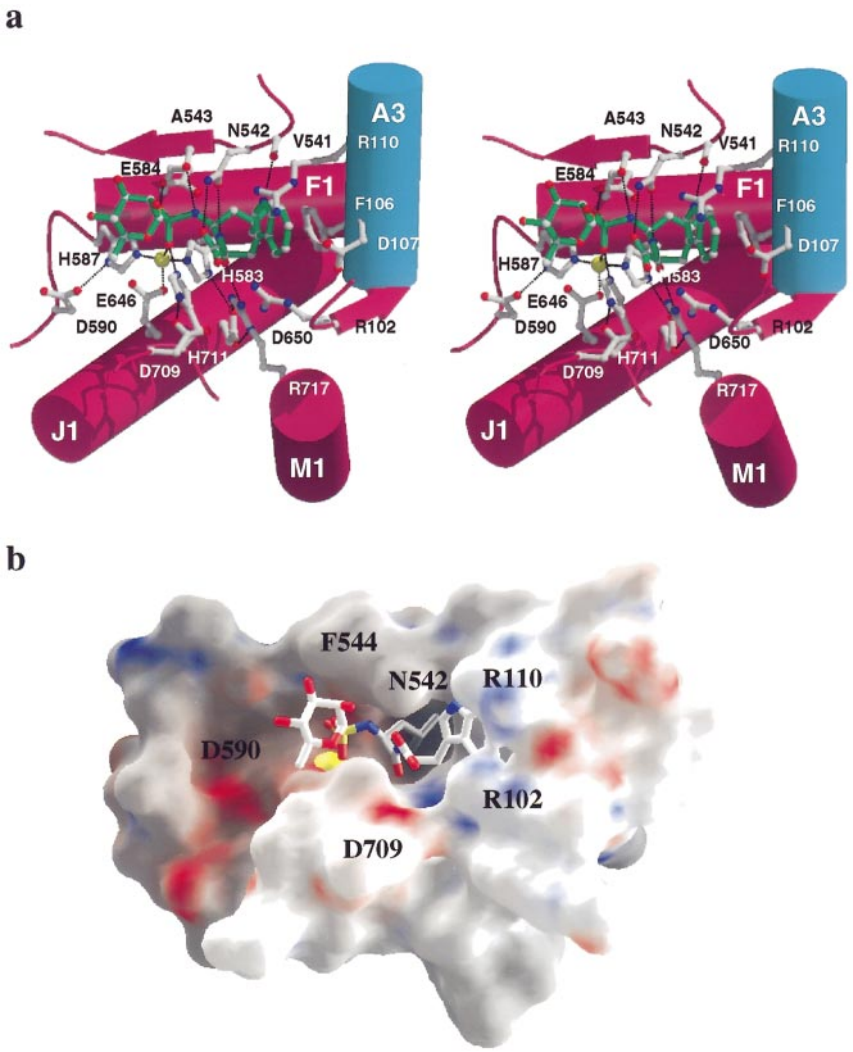


Figure 5. Inhibitor binding to the active site of human sNEP. (a) Stereo view of the active site inhibited by phosphoramidon, green. Hydrogen bonds and ionic interactions are indicated by broken lines, α-helices are shown as cylinders, β-strands are represented by arrows: catalytic domain, violet; the smaller domain 2, blue; the three interdomain linker fragments, cyan. The zinc ion is shown in yellow. (b) Molecular surface of the phosphoramidon recognition site colored by electrostatic potential: positive, blue; negative, red.

Acknowledgments

The authors thank Brigitte D'Arcy and Chantana Yuvaniyama for excellent technical assistance, Beat Wipf for carrying out fermentation experiments and Denise Blum for activity tests. We also thank Neera Borkakoti and Dave Banner for critically reading the manuscript, and Johannes Aebi for continual support.

References

Abassi, Z. A., Tate, J. E., Golombe, E. & Keiser, H. R. (1992). Role of neutral endopeptidase in the metabolism of endothelin. *Hypertension,* **20**, 89-95.

Abrahams, J. P. & Leslie, A. G. W. (1996). Methods used in the structure determination of bovine mitochondrial F1 ATPase. *Acta. Crystallog. sect. A,* **52**, 30-42.

Benchetrit, T., Fournie-Zaluski, M. C. & Roques, B. P. (1987). Relationship between the inhibitory potencies of thiorphan and retrothiorphan enantiomers on thermolysin and neutral endopeptidase 24.11 and their interactions with the thermolysin active site by computer modelling. *Biochem. Biophys. Res. Commun.* **147**, 1034-1040.

Benchetrit, T., Bissery, V., Mornon, J. P., Devault, A., Crine, P. & Roques, B. P. (1988). Primary structure homologies between two Zn-metallopeptidases, the neutral endopeptidase 24.11 ''enkephalinase'' and the thermolysin through clustering. *Biochemistry,* **27**, 592-597.

Brünger, A. T. (1992). Free *R*-value: a novel statistical quantity for assessing the accuracy of crystal structures. *Nature,* **355**, 472-475.

Brünger, A. T., Adams, P. D., Clore, G. M., DeLano, W. L., Gros, P., Grosse-Kunsteleve, R. W., Jiang, J. S., Kuszewski, J., Nilges, M., Pannu, N. S., Read, R. J., Rice, L. M., Simonson, T. & Warren, G. L. (1998). Crystallography & NMR system: a new software suite for macromolecular structure determination. *Acta Crystallog. sect. D,* **54**, 5.

Burnett, J. C. (1999). Vasopeptidase inhibition: a new concept in blood pressure management. *J. Hypertens.* **17**, s37-43.

Chen, H., Noble, F., Coric, P., Fournie-Zaluski, M.-C. & Roques, B. P. (1998). Aminophosphinic inhibitors as transition state analogues of enkephalin-degrading enzymes: a class of central analgesics. *Proc. Natl Acad. Sci. USA,* **95**, 12028-12033.

Collaborative Computational Project No. 4 (1994). The CCP4 suite: programs for protein crystallography. *Acta Crystallog. sect. D,* **50**, 760-763.

de La Fortelle, E. & Bricogne, G. (1997). Maximum likelihood heavy-atom parameter refinement for multiple isomorphous replacement and multiwavelength anomolous diffraction. *Methods Enzymol.* **276**, 472-494.

Devault, A., Lazure, C., Nault, C., LeMoual, H., Seidah, N. G., Chretien, M., Kahn, P., Powell, J., Mallet, J., Beaumont, A., Roques, B. P., Crine, P. & Boileau, C. (1987). Amino acid sequence of rabbit kidney neutral endopeptidase 24. 11 (enkephalinase) deduced from complementary DNA. *EMBO J.* **6**, 1317-1322.

Devault, A., Nault, C., Zollinger, M., Fournie-Zaluska, M.-C., Roques, B. P., Crine, P. & Boileau, G. (1988a). Expression of neutral endopeptidase (enkephalinase) in heterologous COS-1 cells. *J. Biol. Chem.* **263**, 4033-4040.

Devault, A., Sales, N., Nault, C., Beaumont, A., Roques, B. P., Crine, P. & Boileau, G. (1988b). Exploration of the catalytic site of endopeptidase 24.11 by site-directed mutagenesis. Histidine residues 583 and 587 are essential for catalysis. *FEBS Letters,* **231**, 54-58.

Dion, N., Le, Moual H., Crine, P. & Boileau, G. (1993). Kinetic evidence that His-711 of neutral endopeptidase 24.11 is involved in stabilization of transition state. *FEBS Letters,* **318**, 301-304.

Dion, N., Le, Moual H., Fournie-Zaluski, M.-C., Roques, B. P., Crine, P. & Boileau, G. (1995). Evidence that Asn542 of neprilysin (EC 3.4.24.11) is involved in binding of the P2′ residue of substrate. *Biochem. J.* **311**, 623-627.

Emoto, N. & Yanagisawa, M. (1995). Endothelin-converting enzyme-2 is a membrane bound, phosphoramidon-sensitive metalloprotease with acidic pH optimum. *J. Biol. Chem.* **270**, 15262-15268.

Engh, R. & Huber, R. (1991). Accurate bond and angle parameters for X-ray protein refinement. *Acta Crystallog. sect. A,* **47**, 961-963.

Erdos, E. G. & Skidgel, R. A. (1989). Neutral endopeptidase 24.11 (enkephalinase) and related regulators of peptide hormones. *FASEB J.* **3**, 145-151.

Fulcher, I. S., Matsas, R., Turner, A. J. & Kenny, A. J. (1982). Kidney neutral endopeptidase and the hydrolysis of enkephalin by synaptic membranes show similar sensitivity to inhibitors. *Biochem. J.* **203**, 519-522.

Gaucher, J. F., Selkti, M., Tiraboschi, G., Prange, T., Roques, B. P., Tomas, A. & Fournie-Zaluski, M. C. (1999). Crystal structures of α-Mercaptoacyldipeptides in the thermolysin active site: structural parameters for a Zn monodentation or bidentation in metallopeptidases. *Biochemistry,* **38**, 12569-12576.

Gerber, P. (1992). Peptide mechanics: a force field for peptides and proteins working with entire residues as small units. *Biopolymers,* **32**, 1003-1017.

Hersh, L. B. & Morihara, K. (1986). Comparison of subsite specificity of the mammalian neutral endopeptidase 24.11 (enkephalinase) to the bacterial neutral endopeptidase thermolysin. *J. Biol. Chem.* **261**, 6433-6437.

Hoang, M. V., Sansom, C. E. & Turner, A. J. (1997). Mutagenesis of Glu403 to Cys in rabbit neutral endopeptidase-24.11 (neprilysin) creates a disulphide-linked homodimer: analogy with endothelin-converting enzyme. *Biochem. J.* **327**, 925-929.

Jiang, J. S. & Brünger, A. T. (1994). Protein hydration observed by X-ray diffraction. Solvation properties of penicillopepsin and neuraminidase crystal structures. *J. Mol. Biol.* **243**, 100-115.

Kabsch, W. (1988). Evaluation of single crystal X-ray diffraction data from a position sensitive detector. *J. Appl. Crystallog.* **21**, 916-924.

Kenny, A. J. & Stephanson, S. L. (1988). Role of endopeptidase-24.11 in the inactivation of atrial natriuretic peptide. *FEBS Letters,* **232**, 1-8.

Kerr, M. A. & Kenny, A. J. (1974). The purification and specicifity of a neutral endopeptidase from rabbit kidney brush border. *Biochem. J.* **137**, 477-488.

Kim, Y. A., Shriver, B., Quay, T. & Hersh, L. B. (1992). Analysis of the importance of arginine 102 in neutral endopeptidase (enkephalinase) catalysis. *J. Biol. Chem.* **267**, 12330-12335.

Kostrewa, D. (1997). Bulk solvent correction: practicle application and effects in real and reciprocal space. *Joint CCP4 ESF-EACBM Newsletter Protein Crystallog.* **34**, 9-22.

Kraulis, P. J. (1991). MOLSCRIPT: a program to produce both detailed and schematic plots of protein structures. *J. Appl. Crystallog.* **26**, 946-950.

Ksander, G. M., de Jesus, R., Yuan, A., Ghai, R. D., Trapani, A., McMartin, C. & Bohacek, R. (1997a). Ortho-substituted benzofused macrocyclic lactams as zinc metalloprotease inhibitors. *J. Med. Chem.* **40**, 495-505.

Ksander, G. M., Ksander, G. M., de Jesus, R., Yuan, A., Ghai, R. D., Trapani, A., McMartin, C. & Bohacek, R. (1997b). Meta-substituted benzofused macrocyclic lactams as zinc metalloprotease inhibitors. *J. Med. Chem.* **40**, 506-514.

Le, Moual H., Devault, A., Roques, B. P., Crine, P. & Boileau, G. (1991). Identification of glutamic acid 646 as a zinc-coordinating residue in endopeptidase-24.11. *J. Biol. Chem.* **266**, 15670-15674.

Le, Moual H., Dion, N., Roques, B. P., Crine, P. & Boileau, G. (1994). Asp650 is crucial for catalytic activity of neutral endopeptidase 24-11. *Eur. J. Biochem.* **221**, 475-480.

Laskowski, R. A., MacArthur, M. W., Moss, D. S. & Thorton, J. M. (1993). PROCHECK: a program to check the stereochemical quality of protein structures. *J. Appl. Crystallog.* **26**, 283-291.

Lee, S., Zambas, E. D., Marsh, W. L. & Redman, C. M. (1991). Molecular cloning and primary structure of KELL blood group protein. *Proc. Natl Acad. Sci. USA,* **88**, 6353-6357.

Malfroy, B., Schofield, P. R., Kuang, W. J., Seeburg, P. H., Mason, A. J. & Henzel, W. J. (1987). Molecular cloning and amino acid sequence of rat enkephalinase. *Biochem. Biophys. Res. Commun.* **144**, 59-66.

Malfroy, B., Kuang, W.-J., Seeburg, P. H., Mason, A. J. & Schofield, P. R. (1988). Molecular cloning and amino acid sequence of human enkephalinase (neutral endopeptidase). *FEBS Letters,* **229**, 206-210.

Marie-Claire, C., Ruffet, E., Antonczak, S., Beaumont, A., O'Donohue, M., Roques, B. P. & Fournie-Zaluski, M.-C. (1997). Evidence by site-directed mutagenesis that arginine 203 of thermolysin and arginine 717 of neprilysin (neutral endopeptidase) play equivalent critical roles in substrate hydrolysis and inhibitor binding. *Biochemistry,* **36**, 13938-13945.

Matthews, B. (1988). Structural basis of the action of thermolysin and related zinc peptidases. *Acc. Chem. Res.* **21**, 333-340.

Merrit, E. A. & Bacon, D. J. (1997). Raster3D: photorealistic molecular graphics. *Methods Enzymol.* **277**, 505-524.

Nicholls, A. & Honig, B. (1992). *GRASP: Graphical Representation and Analysis of Surface Properties*, Columbia University, New York.

Otwinowski, Z. (1993). Oscillation data reduction program. In *Proceedings of the CCP4 Study Weekend: Data Collection and Processing* (Wawyey, L., Isaacs, N. & Bailey, S., eds), pp. 56-62, SERC Daresbury Laboratory, Daresbury.

Pham, I., El Amrani, A. I. K., Fourne-Zaluski, M. C., Corvol, P., Roques, B. P. & Michel, J. B. (1993). Effects of converting enzyme inhibitor and neutral endopeptidase inhibitor in experimental hypertension. *J. Pharmacol. Exp. Ther.* **265**, 1339-1347.

Robl, J. A., Sun, C.-Q., Stevenson, J., Ryono, D. E., Simpkins, L. M., Cimarusti, M. P., Dejneka, T., Slusarchyk, W. A., Chao, S., Stratton, L., Misra, R. N., Bednarz, M. S., Asaad, M. M., Cheung, H. S. & Abboa-Offei, B. E., *et al*. (1997). Dual metalloprotease inhibitors: mercaptoacetyl-based heterocyclic dipeptide mimetics as inhibitors of angiotensin-converting enzyme and neutral endopeptidase. *J. Med. Chem.* **40**, 1570-1577.

Robl, J. A., Sulsky, R., Sieber-McMaster, E., Ryono, D. E., Cimarusti, M. P., Simpkins, L. M., Karanewsky, D. S., Chao, S., Asaad, M. M., Seymour, A. A., Fox, M., Smith, P. L. & Trippodo, N. C. (1999). Vasopeptidase inhibitors: incorporation of geminal and spirocyclic substituted azepinones in mercaptoacyl dipeptides. *J. Med. Chem.* **42**, 305-311.

Roques, B. P. & Beaumont, A. (1990). Neutral endopeptidase-24.11 inhibitors: from analgesics to antihypertensives? *Trends Pharmacol. Sci.* **11**, 245-249.

Roques, B. P., Fournie-Zaluski, M. C., Soroca, E., Lacomte, J. M., Malfroy, B., Llorens, C. & Schwartz, J. C. (1980). The enkephalinase inhibitor thiorphan shows antiociceptive activity in mice. *Nature,* **288**, 286-288.

Roques, R. P., Noble, F., Dauge, V., Fournie-Zaluski, M.-C. & Beaumont, A. (1993). Neutral endopeptidase 24.11: Structure, inhibition, and experimental and clinical pharmacology. *Pharmacol. Rev.* **45**, 87-146.

Sansom, C., Hoang, M. V. & Turner, A. J. (1998). Molecular modelling and site-directed mutagenesis of the active site of endothelin-converting enzyme. *Protein Eng.* **11**, 1235-1241.

Sheldrick, G. M., Dauter, Z., Wilson, K. S., Hope, H. & Seiker, L. C. (1993). The application of direct methods and Patterson interpretation to high-resolution native protein data. *Acta Crystallog. sect. D,* **49**, 18-23.

Shimada, K., Takahashi, M. & Tanzawa, K. (1994). Cloning and functional expression of endothelin-converting enzyme from rat endothelial cells. *J. Biol. Chem.* **269**, 18275-18278.

Tews, I., Perrakis, A., Oppenheim, A., Dauter, Z., Wilson, K. S. & Vorgias, C. E. (1996). Bacterial chitobiase structure provides insight into catalytic mechanism and basis of Tay-Sachs disease. *Nature Struct. Biol.* **3**, 638-641.

The HYP Consortium (1995). A gene PEX with homologies to endopeptidases is mutated in patients with X-linked hypophosphatemic rickets. *Nature Genet.* **11**, 130-136.

Tiraboschi, G., Jullian, N., Thery, V., Antonczak, S., Fournie-Zaluski, M.-C. & Roques, B. P. (1999). A three-dimensional construction of the active site (region 507-749) of human neutral endopeptidase (EC.3.4.24.11). *Protein Eng.* **12**, 141-149.

Turner, A. J. & Tanzawa, K. (1997). Mammalian membrane metallopeptidases: NEP, ECE, KELL, and PEX. *FASEB J.* **11**, 355-364.

Edited by R. Huber

(Received 4 November 1999; received in revised form 17 December 1999; accepted 17 December 1999)